23rd IMEKO TC4 International Symposium
Electrical & Electronic Measurements Promote Industry 4.0
September 17-20, 2019，Xi'an, China

MV Surge Arresters Monitoring Using Drone Technology

Diego Cavaliere, Alessandro Mingotti, Gaetano Pasini, Lorenzo Peretto, Roberto Tinarelli

Department of Electrical, Electronic and Information Engineering "G. Marconi"
Alma Mater Studiorum – University of Bologna
Bologna, Italy
alessandro.mingotti2, diego.cavaliere2, lorenzo.peretto, roberto.tinarelli3, gaetano.pasini@unibo.it

***Abstract* – This paper presents a pole-mounted measurement system to detect the leakage current of surge arresters. Such a current is a paramount index to determine the aging of the surge arrester. Moreover, all the measurements acquired by the developed pole-mounted system are collected using drones. This way, in every drone flight a huge amount of data can be gathered from the grid. Hence, improving and fastening the power network monitoring and maintenance.**

Keywords – surge arrester, drones, UAV, medium voltage, measurement system, leakage current, pole-mounted system, LoRa, predictive maintenance

I. INTRODUCTION

A paramount element commonly implemented in both transmission and distribution networks is the surge arrester (SA). It is used to protect the network, and in particular all the electrical assets, from overvoltage transients. The causes of such phenomena are multifold: lighting, switching events, faults, etc. As for their manufacture, in the last decades SAs have undergone structural changes, which modified their properties. For example, the resistive part changed from a SiC to a metal oxide (MO) technology. Moreover, the SAs external housing once was made of porcelain while now it is simple silicone material.

Although the improvements reduced the costs and extended the life of the SAs; some drawbacks still affect their life-cycle. As an example, when a SA suffers a fault the silicone housing material do not allow a visual detection of the fault itself (as it was possible with the porcelain one). Hence, utilities operators cannot find and replace the faulted SAs by in-field visual inspection. Furthermore, the constant application of the rated AC voltage on the element is cause of the well-known leakage current, which contribute to the SA aging.

In light of the aforementioned, literature provides several interesting works on the current detection and monitoring of SAs. In [1] the leakage current flowing through the SA is measured by using fiber-optic technology. In [2, 3] instead, a new method to isolate the dangerous leakage current component is provided. In addition, [4, 5] present studies where thermo-cameras images of SAs are combined with the leakage current third harmonic to estimate the "health" status of the arresters.

In this work, authors present a pole-mounted micro-controller-based system, for the leakage current detection in SAs. The measurement system is designed to be mounted on Medium Voltage (MV) poles along with the measurand: the SA. As for the current sensor used, it sends the measurements to the microcontroller which can process them using all the possible frequency-domain techniques.

In addition to that, the system is completed with a fleet of drones capable of acquiring the data collected by the aforementioned acquisition system.

The paper is structured as follows: Section II describes the measurement system, detailing in particular the drones, the pole-mounted acquisition system (PMS) and their communication. All the experimental tests, performed with the proposed system, are listed in Section III. Section IV presents and discusses the obtained results, while some conclusions are drawn in Section V.

II. MEASUREMENT SYSTEM DESCRITPION

The developed test setup used to replicate the normal operation of a SA is shown in Fig. 1. It consists of:

- a programmable power source Agilent 6813B, which features up to 300 V RMS, 1750 VA from DC to 1 kHz. It assures a proper stability for the sinusoidal input voltage applied to the step-up voltage transformer.
- A step-up voltage transformer, which features 15/0.1 kV, 20 VA. Its low voltage terminals are connected to the power source. It rises the output voltage of the power source to the rated voltage of the surge arrester under test.
- The surge arrester under test; its rated voltage and breakdown current are 24 kV and 10 kA, respectively. In addition, it features a salt-proof external shell and an opening device which

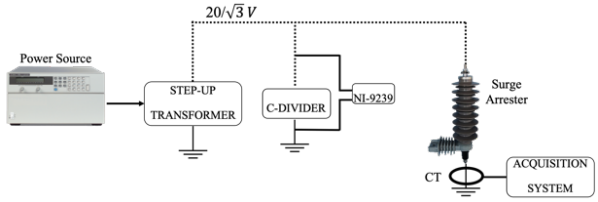

Fig. 1. Simple schematic of the setup for measuring the SA leakage current

Table 1. NORATEL toroidal transformer main characteristics.

Frequency	50 Hz	**Power**	15 VA
Diameter	64.5 mm	**Height**	30.5 mm
Max Ambient Temperature	40 °C	**Accuracy**	1 %

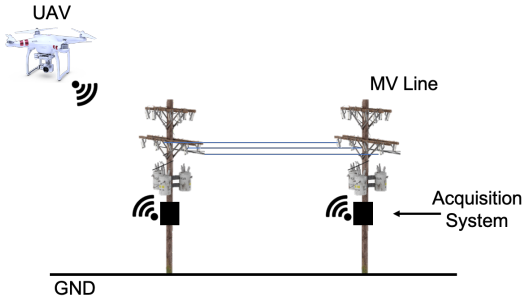

Fig. 2. Schematization of the measurement collection process using the drone

Table 2. XTR-8LR100 communication system technical specification.

Frequency range (1/2)	869.4 – 869.65 MHz	**Frequency range (2/2)**	868 – 868.6 MHz
Size	37x18x2.2 mm	**Channels**	7
Max Emitted Power	100 mW	**Standard distance**	6000 m
Operating Temperature	-20 to +70 °C	**Operating Voltage**	3.3 V

interrupts the circuit in less than 400 ms.

- The pole-mounted acquisition system. It consists of a STM32F411RE microcontroller-based energy meter presented in [6] and briefly recalled in the following. It has been adapted for measurement on SAs and a LoRa®-based communication system has been implemented.
- A capacitive-divider used to reduce the applied voltage for its measurement. It features a nominal ratio of 5981:1.
- A NI9239 24-bit Data Acquisition boards, to measure the actual voltage applied to the SA. It is a ±10 V range DAQ which features: sample rate of 50 kSa/s, gain error of ±0.03 % and offset error of ±0.008 %.
- The current sensor. A NORATEL toroidal transformer TA015/06 used as a current sensor. Its main characteristics are listed in Table 1.
- A laptop for the measurement evaluation and computation.

In Fig. 2 instead, the system for the data collection from the PMS to the drone is depicted. It consists of the UAV and the PMS communicating with the LoRa® technology. In the following subsections, details on the drones, PMS and their communication are provided.

A. Drone Technology and Communication

Unmanned Aerial Vehicles (UAVs) are day by day more integrated in several industrial application, increasing their efficiency and smartness. Different kind of UAV use are listed in [7], including agriculture which has taken lot of advantages [8] from their introduction. Another example is provided by dangerous tasks, as the radioactive source analysis [9], which otherwise could not be performed.

As almost all technology, also UAVs have some drawbacks. In particular, two of them are critical: UAVs cannot flight during bad weather conditions [10] and the Beyond Visual Line Of Sight flight is not possible in many countries or it requires difficult-to-obtain permits.

In light of this, the fleet of drones, provided by Cardtech S.r.l., is composed by a multirotor, a fixed wing and an helicopter. Each kind of UAV adapts to particular requirements of speed, flight duration and flexibility.

To satisfy the measurement requirements of the presented work, they have been equipped with receiver module (RX) of the Aurel XTR-8LR100 transceiver based on SX1276 chipset and LoRa® communication [11, 12]. This solution provides ultra-long-range communication, high interference immunity, high sensitivity and very low power consumption. The transceiver characteristics are listed in Table 2. The transmitter (TX) module system instead, has been installed on the energy meter to complete the communication chain.

B. The PMS

The use of energy meters is spreading along the power networks for several reasons. Among them, there are the increasing penetration of Renewable Energy Sources and the Non-technical losses issue [13-16]. Both reasons obliged DSOs to improve the knowledge of their grid by implementing new energy meters, new distributed measurement systems, and by developing new algorithms [17-20]. The meters must be capable of measuring power and energy either in sinusoidal or of-nominal and distorted conditions.

In light of this, PMS is based on a multifunction energy-meter microcontroller-based developed in [6]. Its

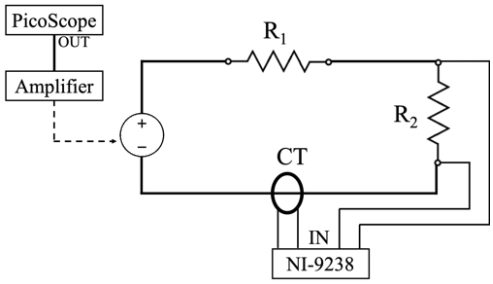

Fig. 3. Schematic of the CT characterization setup

main purpose was to measure the energy in a Low-Voltage (LV) three-phase system. The solution presented in [6] is based on a 32-bit microcontroller which can communicate via I^2C with the energy meter, and via Bluetooth with the external environment. It can operate with 6 channels simultaneously at 8 kSa/s for the current and voltage measurement with an accuracy up to 0.1 %.

In this work, its communication has been enhanced by implementing the LoRa® module. As for the current measurement, in [6] the energy meter was provided with Rogowski coils, while in this work the toroidal transformer – employed as current transformer with voltage output – has been adopted. To maximize the sensitivity of the sensor, the output voltage has been taken from the series of the two 115 V windings.

III. EXPERIMENTAL TESTS

In this Section, three different experimental tests are described: the current sensors characterization, the current measurement on the SA and the communication between the PMS and the drone.

A. PMS - Current sensor characterization

A diagram of the measuring instrument characterization setup is shown in Fig. 3. It consists of:

- the function generator (FG), embedded in the PicoScope 5442D (plus x10 custom amplifier in order to provide the required 1-13 V range), which provides sine wave signals at different frequencies and voltage amplitudes. The frequency range of the FG is 0.025 Hz to 20 MHz and the output voltage is ±2 V;
- a R_1 = 13.5 kΩ resistor in series to the FG, in order to reduce the current magnitude to the range of the one flowing in the ground terminal of the SA;
- a high-accuracy resistor R_2 = 0.5 kΩ obtained from the parallel of two VFR b1739-Z201T 1 kΩ resistors, featuring 0.01 % accuracy;
- the toroidal CT connected to the PMS, used for the SA current measurement.

The test has been done generating 260 different sine wave signals, resulting from the combination of: (i) 20 frequency values (from 50 Hz to 1 kHz, with 50 Hz steps); (ii) 13 voltage amplitudes (from 1 V to 13 V, with 1 V steps). Then, the current flowing through the CT, $\bar{I}_m$, has been obtained by dividing the voltage measured at the high accuracy resistor terminals $\bar{V}_{R2}$ by the resistor itself. As for the CT output, the voltage at its secondary terminals $\bar{V}_{CT}$ has been acquired. Both voltages $\bar{V}_{R2}$ and $\bar{V}_{CT}$ have been acquired by two input channels of the 24-bit NI9238 Data Acquisition board at 50 kSa/s, 1 s time record. The NI9238 is a ±0.5 V range DAQ which features: sample rate of 50 kSa/s, gain error of ±0.07 % and offset error of ±0.005 %. For each of the 260 input signals, 30 measurement have been collected.

By adopting the same setup presented in Fig. 3, an additional characterisation has been done. In particular, to consider the possible lower amplitudes of the third harmonic component in the SA leakage current, the resistors values have been changed. In other words, the characterisation has been repeated with R_1 = 10 MΩ and R_2 = 1 kΩ, 0.01 % accuracy.

B. Current measurements

By using the setup of Fig. 1, the leakage current of the SA has been measured. The power source fed the step-up transformer to obtain up to $20/\sqrt{3}$ kV voltage applied on the SA. This value has been chosen since it is the typical nominal value for line-to-line voltage in Italian distribution networks. The voltage is reduced and measured by mean of capacitive-divider and the DAQ, respectively. Afterwards 30 measurements of CT output voltage, to compute the leakage current, have been acquired.

C. Wireless Communication Test

To test the communication between the PMS (TX) and the drone (RX), the RX has been moved along a track in urban/semi-urban landscape, while its geographical position has been tracked with a GPS. The goal of the test was to validate the quality of the data transmission when the distance and the relative speed between the RX and TX is varying. Therefore, a telegram containing a data payload of 250 bytes has been cyclically sent to RX, using a 1-second cycle. The quality of the communication has been assessed by means of a byte error ratio (BER), for each received packet, defined by the authors as:

$$BER = \frac{number\ of\ byte\ errors}{total\ number\ of\ received\ bytes}\%. \qquad (1)$$

IV. EXPERIMENTAL RESULTS

A. PMS - Current sensor characterization results

Results of both the characterisation test, in terms of measured reference current, are listed in Table 3. It contains the mean values $\tilde{I}_m$ of $\bar{I}_m$ and their associated uncertainty u_I for the two frequencies of interest, 50 Hz and 150 Hz.

Fig. 4 and Fig. 5 show the ensemble of parametric

Table 3. Mean values and uncertainty of the reference current $\bar{I}_m$ for the two frequencies of interest (50 Hz and 150 Hz).

	Frequency [Hz]			
	50		*150*	
Test Voltage [V]	$\tilde{I}_m$ [µA]	u_I [µA]	$\tilde{I}_m$ [µA]	u_I [µA]
1	49.12	0.05	0.35	0.01
2	98.31	0.07	0.71	0.01
3	147.36	0.09	1.06	0.01
4	196.5	0.1	1.41	0.02
5	245.6	0.1	1.76	0.02
6	294.6	0.2	2.11	0.02
7	343.7	0.2	2.47	0.02
8	392.8	0.2	2.82	0.02
9	442.0	0.2	3.17	0.02
10	491.1	0.2	3.52	0.02
11	540.2	0.3	3.87	0.02
12	589.3	0.3	4.22	0.02
13	638.1	0.3	4.58	0.02

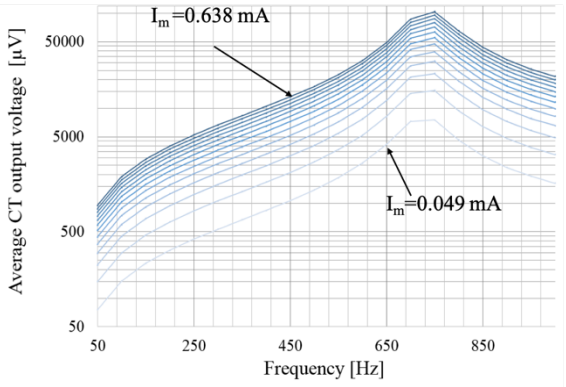

Fig. 4. CT ouput voltage vs. frequency in light of the parameter $\bar{I}_m$ value. Case: R_1 = 13.5 kΩ and R_2 = 0.5 kΩ.

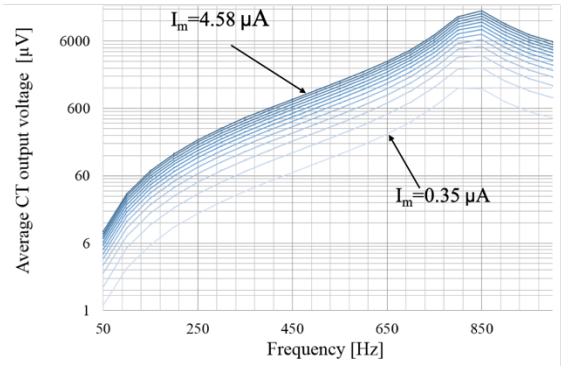

Fig. 5. CT ouput voltage vs. frequency in light of the parameter $\bar{I}_m$ value. Case: R_1 = 10 MΩ and R_2 = 1 kΩ.

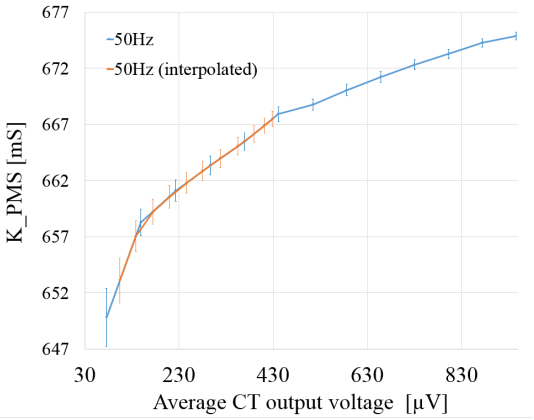

Fig. 6. K_{PMS} at 50 Hz obtained from the characterization (blue curve) and the interpolation (orange curve).

curves representing the average CT output voltage $\tilde{V}_{CT}$ plotted against frequency. The former refers to the high-current range (obtained with R_1 = 13.5 kΩ and R_2 = 0.5 kΩ), while the latter refers to the low-current range, specific for the third harmonics (R_1 = 10 MΩ and R_2 = 1 kΩ). In both Figures the parameter is the current $\bar{I}_m$ and it can be noticed that:

- the higher the current, the higher the curve, denoting a monotonic behaviour of $\tilde{V}_{CT}$. In particular, the latter ranges from (about) 76 µV to 950 µV at 50 Hz (in Fig. 4) and from 6 µV to 72 µV at 150 Hz (in Fig. 5).
- the measurement device under test reaches its peak sensitivity in correspondence of 750 Hz in Fig. 4 and of 850 Hz in Fig. 5.

To preliminary evaluate the $\tilde{V}_{CT}$ measurement goodness, the related standard deviation of the mean σ_{VC} has been computed. Results confirms that little variations of the quantities of interests can be detected with the proposed setup. As a matter of fact, for all the current values within the measured range, all the computed σ_{VC} where below 1 µV and 0.1 µV, for the cases of Fig. 4 and Fig. 5, respectively. This holds for both the frequencies of interest, 50 and 150 Hz, while in the 700 – 850 Hz range the highest dispersion of the measurement is experienced.

Once the σ_{VC} has been evaluated, it has been possible to compute the transfer function of the presented measurement device. This quantity has been named K_{PMS} and defined as the ratio of the primary current ($\bar{I}_m$) to the output voltage ($\bar{V}_{CT}$), as follows:

$$K_{PMS} = \frac{\bar{I}_m}{\bar{V}_{CT}} \qquad (2)$$

The average value K_{PMS}, referred to as $\tilde{K}_{PMS}$, and its uncertainty u_K have been computed from the quantities measured in the characterization test. They are displayed as the blue curves in both Fig.6, for 50 Hz, and in Fig. 7,

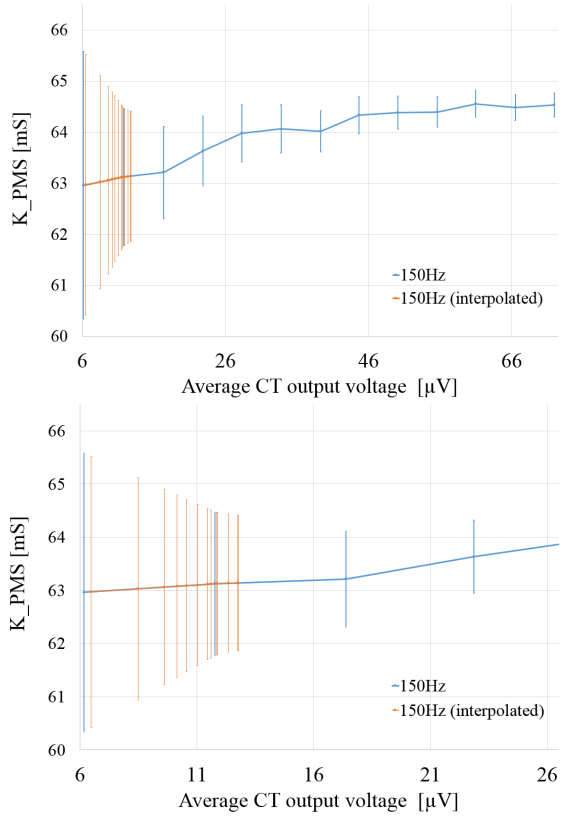

Fig. 7. K_{PMS} at 150 Hz obtained from the characterization measurements (blue curve) and the interpolation (orange curve).

Table 4. Mean values and standard deviations of $\bar{I}_{Leak}$ for the two frequencies of interest (50 Hz and 150 Hz).

	Frequency [Hz]			
	50		***150***	
Test Voltage [kV]	$\tilde{I}_{Leak}$ **[µA]**	u_{IL} **[µA]**	$\tilde{I}_{Leak}$ **[µA]**	u_{IL} **[µA]**
3	68.2	0.2	0.57	0.02
4	91.2	0.2	0.60	0.02
5	114.9	0.2	0.63	0.02
6	138.2	0.2	0.66	0.03
7	162.6	0.2	0.69	0.03
8	186.0	0.3	0.71	0.03
9	210.7	0.3	0.69	0.03
10	236.0	0.3	0.71	0.04
11	259.6	0.3	0.74	0.04
11.55	274.4	0.3	0.77	0.04
12	285.9	0.3	0.77	0.04

for 150 Hz. In both figures, it can be highlighted that the toroidal transformer is working with a very low primary current, hence in correspondence of an operating point in

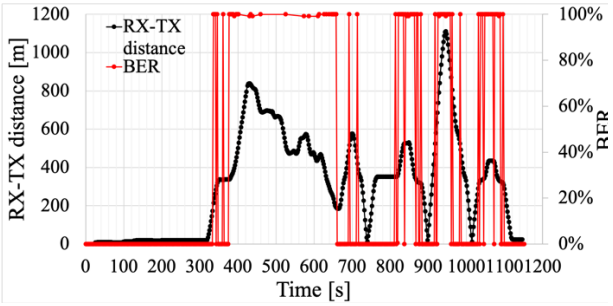

Fig. 8. BER and distance between RX and TX plotted against time

the very beginning of the B-H iron curve. Hence, implying a predominant magnetization current contribution. In Fig. 7, the upper graph represents the entire range of measurements performed during the characterization process. Instead, in the lower graph a zoom over the interest range is presented.

B. Current measurement

Once the transfer function K_{PMS} is known, the leakage current $\bar{I}_{Leak}$ flowing through the SA can be computed by starting from the measured voltage $\bar{V}_{CT}$ at the CT terminals. To compute the conversion, and for each measured voltage, the $\tilde{K}_{PMS}$ has been interpolated in correspondence of the measured $\tilde{V}_{CT}$; then its associated uncertainty u_K has been computed. Obtained values are displayed as orange curves in both Fig. 6 and Fig. 7, for 50 Hz and 150 Hz, respectively.

Finally, by means of (2) the leakage currents have been computed and listed in Table 4. It contains the mean values $\tilde{I}_{Leak}$ of the current along with their associated uncertainty u_{IL} for both the frequency of interest, 50 and 150 Hz.

The results presented in paragraphs *A.* and *B.* above suggest that the presented measurement device equipped with the CT is suitable to be employed as a monitoring device for the leakage current of MV surge arresters across the distribution network. However, given the magnitude of the CT output voltage, a proper signal conditioning is needed for the on-site deployment, which will be further analysed in future work.

C. Wireless Communication test results

Fig. 8 shows the results of the communication test. It consists of two curves: the dotted one is the distance between the moving RX and the fixed TX against time. The solid one instead, is the computed BER during the RX movement along the chosen urban/semi-urban track. From the graph, three considerations arise: (i) during the time interval 350-650 s the communication was severely impaired due to presence of many buildings in "Line of Sight" path between the RX and TX. (ii) if the RX-TX distance is greater than 300 m, then the communication cannot be considered reliable in the considered landscape. This does not compromise the proposed solution because

the drone will fly far closer to the PMS than 300 m (max tens of meters). (iii) the RX's relative speed was 70 km/h at 900 s, this means that LoRa® modulation is capable to withstand transmission when RX and TX are moving at such a relative speed. In light of this last comment, fixed-wing drones can be conveniently operated at 70 km/h and, in MV overhead line monitoring application, the drone shall overfly the line at a 30-40 m altitude, with no obstacles in the middle. The experimental results show that the low-power communication modules under test are a very valid solution for the presented application.

V. CONCLUSIONS

The use of drones in the power engineering industry is increasing day by day. Several applications use this technology to improve processes and to implement new features to existing ones. With this aim, in this paper a measurement system composed by an UAV and by an acquisition system has been developed and tested. In particular, tests have been performed on a critical medium voltage accessory: the surge arrester. The developed system allows to measure the leakage current flowing through the surge arrester. Afterwards a drone may collect all the measurement from the acquisition system with the communication tested in the work. Presented results confirm the efficiency and accuracy of both the developed acquisition system and its communication system.

VI. AKNOWLEDGMENT

Authors would like to thank Cardtech S.r.l. for providing the fleet of drone used in the paper and all the support necessary for their correct operation and piloting.

REFERENCES

[1] T. Taskin, "Introduction of a measurement system to monitor the condition of ZnO surge", IEEE Power Engineering Society Winter Meeting, Singapore, Jan. 2000.

[2] S. M. Arshad, A. S. Rodrigo, "Modified phase shifting of leakage current to condition monitoring of metal oxide surge arresters in power system", Moratuwa Engineering Research Conference, Moratuwa June 2018.

[3] Z. Abdul-Malek, N. Yussof, M. F. M. Yousof, "Field experience on surge arrester condition monitoring – Modified shifted current method", International Universities Power Engineering Conference, Sept. 2010.

[4] H. Kayan, R. Eslampanah, F. Yeganli, M. Askar, "Heat leakage detection and surveillance using aerial thermography drone", Signal processing and Communications Applications Conference, Izmir, May 2018.

[5] Novizon, Z. Abdul-Malek, "Electrical and temperature correlation to monitor fault condition of ZnO surge arrester", International Conference on Information Technology, Computer, and Electrical Engineering, Semarang, Oct. 2016.

[6] L. Bartolomei, A. Mingotti, G. Pasini, L. Peretto, P. Rinaldi, R. Tinarelli, L. Puddu, "Performance evaluation of an energy meter for low-voltage system monitoring", International Measurement Confederation, Belfast, Sept. 2018.

[7] P. Daponte, L. De Vito, G. Mazzilli, F. Picariello, S. Rapuano, M. Riccio, "Metrology for drone drone for metrology: measurement systems on small civilian drones", IEEE Metrology for Aerospace, Benevento, June 2015.

[8] F. N. Murrieta-Rico, D. Hernandez-Balbuena, J. C. Rodriguez-Quinonez, V. Petranovsk et all, "Resolution improvement of accelerometers measurement of drones in agricultural applications", Annual Conference of the IEEE Industrial Electronics Society, Oct. 2016.

[9] J. Baeza, D. Valencia, A. Baeza, "Use of drones for remote management of the close measure of radioactivity sources", IEEE International Geoscience and Remote Sensing Symposium, Valencia, July 2018.

[10] S. S. Altman, V. Vulfin, H. Leibovich, R. Heinrich, R. Ianconescu, "Lighting strike analysis for drones", IEEE International Conference on Microwaves, Antennas, Communications and Electronic Systems, Tel-Aviv, Nov. 2017.

[11] Patent EP2763321 – Low power long range transmitter.

[12] Patent US7791415B2 – Fractional-N synthesized chirp generator.

[13] L. Bartolomei, A. Mingotti, L. Peretto, P. Rinaldi, "Accuracy Verification of PLL-Based Acquisition System for Low-Cost Applications", IEEE 9th International Workshop on Applied Measurements for Power Systems Bologna, Sept. 2018.

[14] N. Constandache, D. M. Stanescu, M. Sanduleac, C. Stanescu, I. Tristiu, A. Mandis, "Smart Meters, PMU and PQ data analysis in Active Distribution Grids – Case Studies in MV networks", International Conference on Applied and Theoretical Electricity, Craiova, Oct. 2018.

[15] A. I. Lita, D. A. Visan, M. Gherghe, L. M. Ionescu, A. G. Mazare, I. Lita, "Microcontroller Based Magnetometer for Smart Meters Used in Electrical Energy Measurement", International Spring Seminar on Electronics Technology, Zlatibor, May 2018.

[16] M. Armendariz, D. Babazadeh, L. Nordström, M. Barchiesi, "A method to place meters in active low voltage distribution networks using BPSO algorithm", Power Systems Computation Conference, Genoa, June 2016.

[17] J. B. Leite, J. R. Sanches Mantovani, "State estimation of distribution networks through the real-time measurements of the smart meters", IEEE Grenoble Conference, Grenoble, June 2013.

[18] A. Mingotti, L. Peretto, R. Tinarelli, "Accuracy Evaluation of an Equivalent Synchronization Method for Assessing the Time Reference in Power Networks", *IEEE Transactions on Instrumentation and Measurement*, vol. 67, no. 3, pp. 600-606, 2018

[19] K.V.S. Baba, S.R. Narasimhan, N.L. Jai, A. Singh, R. Shukla, A. Gupta, "Synchrophasor based real time monitoring of grid events in Indian power system", IEEE International Conference on Power System Technology, Wollongong, Australia, Oct. 2016.

[20] A. Mingotti, L. Peretto, R. Tinarelli, A. Angioni, A. Monti, F. Ponci, "Calibration of synchronized measurement system: from the instrument transformer to the PMU", IEEE 9th International Workshop on Applied Measurements for Power Systems, Bologna, Italy, Sept. 2018.